



Synergistic Insights into the Structural, Optical, and Magnetic Features of Iron-Modified Tin Oxide (Fe-SnO₂) Nanoparticles: An Integrated Experimental and First Principles Investigation

Pawan Chetri¹  · Nishant Shukla²

Received: 3 October 2023 / Accepted: 26 February 2024 / Published online: 13 March 2024
© The Author(s) under exclusive licence to Sociedade Brasileira de Física 2024

Abstract

The synthesis of SnO₂ nanoparticles doped with varying concentrations of Fe was carried out using the sol–gel method. The resulting samples underwent analysis using X-ray diffraction (XRD), high-resolution transmission electron microscopy (HR-TEM), ultraviolet–visible spectroscopy (UV–Vis), diffuse reflectance spectroscopy (DRS), photoluminescence spectroscopy, and vibrating sample magnetometry. The purpose of this investigation was to examine the impact of doping on the structural, optical, and magnetic properties of the nanoparticles. The XRD study demonstrated a discernible alteration in the size of the crystalline structure as a function of the concentration of doping. The study revealed a noticeable variation in crystallite size, ranging from ~ 13 to 5 nm, as the Fe doping concentration increased from 0 to 7 mol%. This observation suggested that the rise in Fe content effectively hindered crystal development. The estimation of the optical band gap was performed using the Kubelka–Munk equation, revealing a decrease in the band gap for a specific doping concentration of Fe. The photoluminescence (PL) spectra obtained at room temperature indicated a red shift in the peak positions of the pristine SnO₂ samples upon Fe doping. This observation provides confirmation of the reduction in the band gap of SnO₂ resulting from the incorporation of Fe dopants. The nanoparticles doped with 5% Fe exhibited superior optical characteristics compared to the remaining samples. Furthermore, magnetic properties were determined by investigating magnetization vs. applied fields. Ferromagnetic interaction was observed in all the systems of SnO₂ doped with Fe. To achieve a comprehensive understanding, the utilization of density functional theory was employed. The electronic states and density of states behavior were computed to accurately anticipate the arrangement of lattice sites and the corresponding presence of atoms. Theoretical computations were conducted using the VASP program.

Keywords SnO₂ · XRD · TEM · UV–Visible · Magnetic property · DFT

1 Introduction

The scientific community increasingly recognizes the importance of synthesizing nanomaterials for both pure and practical research. This recognition arises from the fact that material properties undergo significant changes when scaled down to the nanoscale range [1]. These characteristics

hold considerable promise for practical applications, and in recent times, extensive investigations have been conducted into the optical and magnetic attributes of nanocrystalline semiconductors. Presently, there is considerable interest in nanostructures composed of SnO₂ due to its potential utilization in fields such as light-emitting and light-triggered semiconductor devices, detectors, flat panel displays, solar cell arrays, heated windows, anti-static coatings, solid-state gas sensors, surge arrestors (varistors), and oxidation catalysts [2–7]. The extraordinary combination of transport and optical properties in SnO₂ is attributed to the simultaneous presence of oxygen vacancies and tin interstitials [8, 9].

In contemporary times, researchers have found ferromagnetic semiconductors to be a compelling area of study. Non-magnetic semiconductors can be rendered magnetic through the process of doping with magnetic impurities while still

✉ Pawan Chetri
chetripawan2009@gmail.com

✉ Nishant Shukla
shukla.coolnishu@gmail.com

¹ Dept of Physics, Debraj Roy College, Golaghat, India

² Dept. of Applied Sciences, HMR Institute of Technology and Management, Delhi, India

maintaining their semiconducting characteristics. Pure SnO_2 often requires alterations to enhance various properties, including conductivity, optical absorption, gas sensitivity, and magnetic properties. These modifications can be achieved through a process known as doping [10–12]. In a recent study, it has been discovered that the introduction of iron (Fe) doping into titanium dioxide (TiO_2) enhances its photocatalytic properties, surpassing those of pure TiO_2 [13, 14]. This finding demonstrates that the introduction of Fe doping significantly enhances the photocatalytic activity of oxide materials. Iron (Fe) is an element with magnetic properties, and when it is incorporated into tin dioxide (SnO_2), it imparts magnetic characteristics to the compound. The impurity employed to induce magnetic properties has a low concentration, typically a few percent, classifying it as a dilute magnetic semiconductor. The inclusion of Fe in SnO_2 results in an enhanced intrinsic magnetic characteristic, hence classifying it as a Dilute Magnetic Semiconductor (DMS) [15].

In the present study, Fe dopants have been introduced into tin dioxide (SnO_2) at varying concentrations of 3%, 5%, and 7%. Subsequently, the influence of these dopants was investigated on the structural, optical, and magnetic characteristics of the doped SnO_2 material. The introduction of iron (Fe) doping has resulted in significant alterations in the structural characteristics of tin dioxide (SnO_2), impacting its optical qualities. The exploration for the development of high-temperature ferromagnetic semiconductors began with the investigation of SnO_2 as one of the candidate materials. The precise cause of room temperature ferromagnetism remains uncertain, despite postulated mechanisms including the creation of magnetic polarons and exchange interactions driven by defects [16–18]. In this study, Fe-doped SnO_2 samples were synthesized with varying concentrations, and their magnetic properties were investigated through the measurement of magnetization as a function of the magnetic field. A Density Functional Theory (DFT) simulation was also conducted to investigate the atomistic-level modifications in the characteristics of Fe-doped SnO_2 in comparison to pure SnO_2 .

2 Experimental and Computational Details

2.1 Synthesis of Pristine and Fe Doped SnO_2 Nanoparticles

The synthesis of pristine SnO_2 nanoparticles began with the addition of 1 gm of $\text{SnCl}_2 \cdot 2\text{H}_2\text{O}$ to a mixture containing 11 ml of deionized water and 5 ml of ethanol. The resulting solution was stirred for 5 min, followed by the gradual addition of 1 ml of HCl. After an additional 15 min of stirring, the solution's pH was adjusted to 10 by the dropwise

addition of aqueous ammonia. This pH-adjusted solution was stirred for 2–3 h at 80 °C. The outcome was a grayish solution, which underwent washing with deionized water and ethanol to obtain SnO_2 nanoparticles free from impurities, particularly chlorine. Subsequently, it was annealed at 450 °C. The Fe-doped SnO_2 nanoparticle was prepared by adding a dropwise solution of $\text{FeCl}_3 \cdot 5\text{H}_2\text{O}$. Fe was doped at three different concentrations: 3%, 5%, and 7% to form $\text{Sn}_{1-x}\text{Fe}_x\text{O}_2$, where $x = 0.03, 0.05,$ and 0.07 , respectively.

2.2 Characterization and Computational details

The phase structures of the nanoparticles were examined using a Rigaku Miniflex X-ray diffractometer equipped with intense $\text{CuK}\alpha$ radiation ($\lambda = 1.54 \text{ \AA}$), at a scanning rate of 10/min and in the scanning range from 100–700. High-resolution transmission electron microscope (HRTEM) images of the prepared nanoparticles were captured with a JEOL JEM 2010 transmission electron microscope operating at a voltage of 200 kV. UV–Vis absorption spectra of all SnO_2 nanoparticles were recorded in diffuse reflectance mode (DRS) using a Shimadzu 2450 UV–Vis spectrophotometer. Photoluminescence (PL) spectra were monitored in a Perkin Elmer LS spectrometer. The EDS pattern was obtained from a JEOL JSM Model 6390 LV. The variation of the magnetic moment with the applied field at room temperature and the variation of the magnetic moment with temperature were measured by vibrating sample magnetometry. To examine the interaction between two Fe atoms, the second Fe atom was placed in three different positions, and the magnetic properties of the system were investigated.

A $2 \times 2 \times 2$ supercell was constructed using the unit cell of SnO_2 in the rutile form, with the initial space group of pure SnO_2 being set as P42/mnm. The introduction of Iron (Fe) into the SnO_2 system involved replacing one central tin (Sn) atom with a Fe atom, resulting in a reduction of symmetry to P1. This adjustment ensured that the system was free from any symmetry constraints. Subsequently, all atoms were allowed to relax in all directions to achieve the minimum energy configuration. The theoretical calculations were conducted using the generalized gradient approximation (GGA) functional with the Perdew–Burke–Ernzerhof (PBE) model to account for electron–electron exchange and correlation effects. The density functional theory (DFT) equations were solved using the projector augmented wave method with a plane wave basis set, implemented in VASP and interfaced with the MedeA technology platform. The minimum energy state was computed by adjusting the internal positions of atoms until the residual force was 0.01 eV/Å. A cutoff energy of 480 eV was employed for expanding the electronic wave-functions. Geometry optimizations and electronic property calculations involved Brillouin-zone integration, performed using a $3 \times 3 \times 5$ Monkhorst–Pack k-point

grid. In the magnetic study, two Fe atoms were considered within the mentioned supercell. To examine the interaction between these two Fe atoms, the second Fe atom was placed in three different positions, and the system's magnetic properties were investigated. For the density of states calculation denser values of $16 \times 16 \times 16$ k-points were employed. The Broyden-Fletcher-Goldfarb-Shanno algorithms were used for geometry relaxation calculations as a consequence of the Born–Oppenheimer approximations. Real space projection operators were used instead of reciprocal space projection due to the system's large number of atoms.

3 Results and Discussion

3.1 Structural Characterization

The structural properties of all the prepared samples were investigated using XRD, as shown in Fig. 1. The diffraction peak of all the samples corresponds to the rutile phase of SnO₂ (JCPDS 41–1445). The detailed analysis of crystal planes can be found in [19]. No phase of foreign compounds like

Table 1 System, crystallite size and band gap

System	Crystallite Size (nm)	Band gap (eV)
SnO ₂	12.50	3.91
Fe3% SnO ₂	4.66	3.83
Fe5% SnO ₂	4.27	3.35
Fe7% SnO ₂	5.03	3.84

FeO or Fe₂O₃ was observed, implying that Fe has not formed any clusters, and most of the Fe atoms substituted Sn at its lattice site. The average crystallite size was calculated using Scherer's equation,

$$d = \frac{0.91 \lambda}{\beta \cos \Theta} \tag{1}$$

The calculated values are listed in Table 1. The plot of crystallite size vs doping concentration (x), as shown in Fig. 1(b), indicates that as x increases, the crystallite size decreases. The lowest value is obtained for x = 5. The Fe present in the system can be in two different charge states, i.e., Fe²⁺ or Fe³⁺. When Fe is incorporated within SnO₂, it

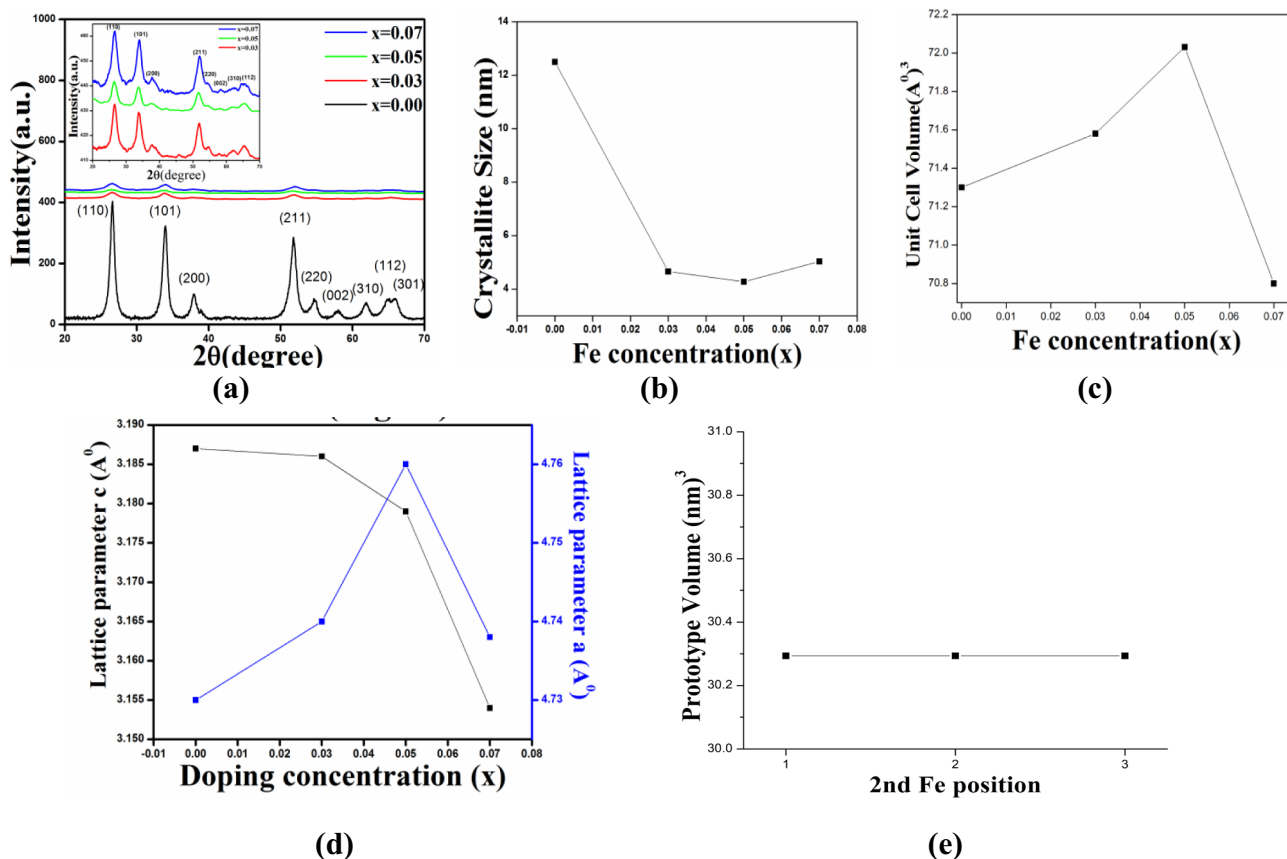


Fig. 1 (a) X-ray diffraction of all the prepared samples. (b) Crystallite Size Vs Fe concentration (x) (c) Lattice parameter Vs. doping concentration (x) and (d) Unit cell volume Vs Fe concentration (e) volume optimization curves for different structure prototype

substitutes Sn^{4+} and Sn^{2+} present in the system. Except for size difference, when Fe^{2+} substitutes Sn^{2+} , then there would be no generation of O vacancies as the charge state of both cations is the same. But in all other cases, i.e., Fe^{2+} substituting Sn^{4+} and Fe^{3+} substituting Sn^{2+} or Sn^{4+} , charge imbalance occurs. This charge imbalance is relieved by forming O vacancies. The substitution of Fe in SnO_2 and consequent formation of O vacancies lead to defects in the system and hence crystallite size decreases. This reduction in crystallite size with Fe doping has also been observed previously [20, 21]. Furthermore, Fe^{3+} ion has a smaller radius (0.055 nm) than Sn^{4+} ion (0.071 nm), so SnO_2 doping with Fe^{3+} should result in the contraction of the lattice parameters, leading to a decrease in crystallite size. The lowest value of crystallite size for $x=5$ might be due to the high number of defects present in the system. The lattice parameters (a and c) and unit cell volume are calculated and plotted vs. x as shown in Fig. 1(c-d) respectively. The lattice parameter c decreases as x increases, while the lattice parameter a increases up to $x=5$ and then decreases. The unit cell volume also increases up to $x=5$ and then decreases. As the defects increase in the system, it tends to expand the unit cell to relax the structure. From Fig. 1(b), it appears that $x=5$ has the highest number of defects, so the largest value of its unit cell is obvious. The smallest size of the Fe 5% SnO_2 nanosystem signifies that it contains a high number of defects and the maximum of Fe has substituted lattice Sn sites. In Fe 7%, the crystallite size increases compared to Fe 5%, and it might be because all the dopant Fe has not substituted Sn lattice sites and remained as interstitial. As there is less substitution, lesser charge imbalance occurs, and a smaller number of oxygens vacancies form. Fe atoms sitting in the interstitial will not affect the lattice to decrease their crystallite size. High resolution TEM image of Fe 7% doped SnO_2 is presented in Fig. 2. The high amount of mismatched lattice planes can be seen in Fe 7% doped SnO_2 system.

Fig. 2 High resolution TEM of (a) Pristine SnO_2 (b) Fe 7% doped SnO_2

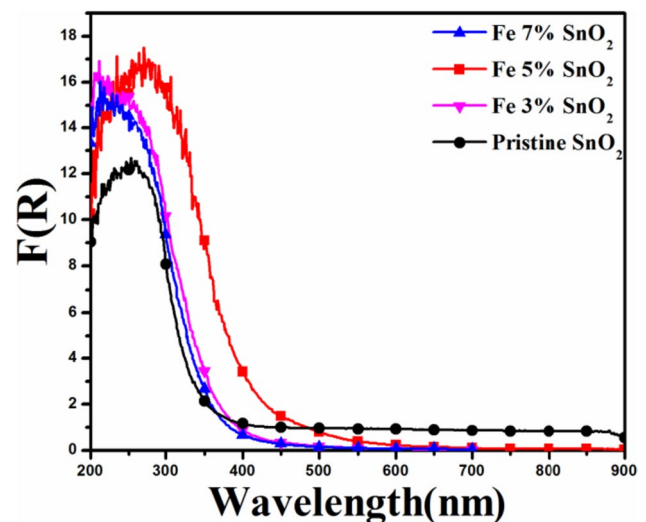
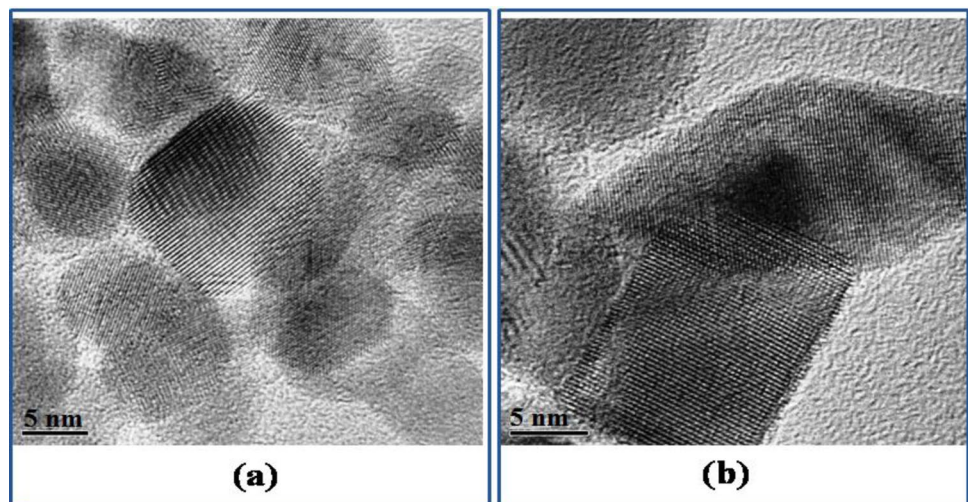


Fig. 3 $F(R)$ Vs Wavelength of all the prepared systems

3.2 Optical Characterization

To have a better understanding of the effect of dopant (Fe) and the defects on optical properties of SnO_2 nanoparticles, UV–Visible spectroscopy was performed. The absorbance is given by:

$$F(R) = \frac{(1 - R)^2}{2R} \quad (2)$$

The variation of absorbance with the wavelength of all the samples is shown in Fig. 3. Figure 4 shows the band gap of all the systems. The band gap is calculated using the Kubelka–Munk equation, where $[F(R) h\nu]^2 = 0$ is plotted against incident photon energy $h\nu$, and the extrapolated line at $[F(R) h\nu]^2 = 0$ gives the value of the band gap in eV. The band gap value of all the samples is listed in Table 1.

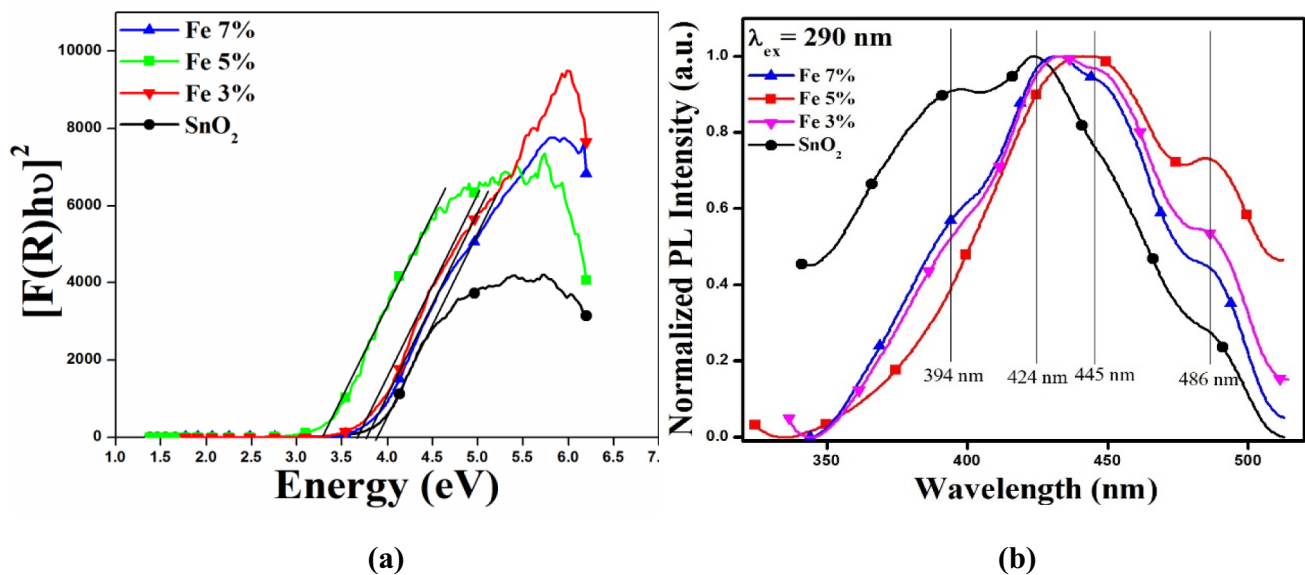


Fig. 4 (a) Band gap calculation (b) Photoluminescence spectra of all the prepared systems

Pure SnO_2 is found to have a band gap of 3.91 eV. Fe doping somehow reduces the band gap. A high amount of band gap reduction can be seen for Fe 5% doped SnO_2 . On the other hand, Fe 3% and Fe 7% have almost the same value of the band gap. This red shifting of the band gap can be due to the incorporation of Fe^{3+} into the SnO_2 crystal structure [22, 23], which leads to the charge-transfer transition between the Fe^{3+} d-electrons and the SnO_2 conduction or valence band. The reduction in the band gap can also be due to the creation of oxygen vacancies. These oxygen vacancies due to their high concentrations create levels within the band gap, forming a virtual band near the bottom of the conduction band, and thus decreasing the band gap. The effect of oxygen vacancies on the band gap might have played a role in Fe 5% SnO_2 . From XRD, we have seen that in Fe5% SnO_2 , higher substitution of Fe took place, which indirectly formed a greater number of oxygen vacancies. Thus, we predict that the substitution of Fe in the Fe 5% SnO_2 system enables a greater number of oxygen vacancies, leading to an abnormal decrease in the band gap.

Photoluminescence spectroscopy, as shown in Fig. 4(b), was done to check the effect of Fe doping on the luminescence property of SnO_2 nanoparticles. Peak 0 to 1 was normalized such that shifting in Fe-doped samples with respect to the pristine SnO_2 can be understood. Band-edge emission was not observed in any of the samples, which might be due to the detection limit of the instrument. The pristine SnO_2 nanoparticle shows peaks at 394, 424, 445, and 486 nm. Fe doping has red-shifted all the peaks apart from the peak at 486 nm of pristine SnO_2 . Thus, confirming the reduction in the band gap of SnO_2 . The first peak of pristine SnO_2 at 394 nm may reflect the below conduction band absorption (but not the band edge absorption), while other peaks are due

to oxygen vacancies. In the case of Fe 5% SnO_2 , we have observed only 3 peaks, and the peak observed in pristine SnO_2 at 394 nm is absent. The absence of this peak can be due to the presence of different states near the bottom of the conduction band. These different states are formed due to the presence of Fe in substituted sites and the oxygen vacancies. The concentration of these states is so high that it completely quenched the emission observed at 394 nm in pristine SnO_2 . This peak appeared in the Fe 3% and Fe 7% SnO_2 systems. As was already discussed, the effect of Fe doping is not prominent in the Fe 3% and Fe 7% SnO_2 systems. In both systems, it was seen from XRD and UV–Visible spectroscopy that complete substitution of Fe did not take place.

3.3 Magnetic Properties Study

Magnetic measurements were performed for all the systems as shown in Fig. 5(a). All the prepared samples including pristine SnO_2 show ferromagnetic interaction. From M-H curve it can be observed that there are spins which are not aligned along the direction of applied field (high field). The decreased ferromagnetism observed for Fe 7% can be due to the competitive effects of ferromagnetic and antiferromagnetic interaction. The variation of magnetic property with temperature for $\text{Sn}_{0.93}\text{Fe}_{0.05}\text{O}_2$ is observed in both ZFC and FC condition. No humps or peaks are observed in the ZFC–FC curve confirming the presence of moments even at a very low temperature and no formation of FeO or Fe_2O_3 phase. The M-T curve is taken at 200 Oe and the bifurcation of ZFC–FC curve up to 300 K ensures that the system remains ferromagnetic at temperatures 300 K. The bifurcation between ZFC and FC curve at 200 Oe indicates a ferromagnetic behavior.

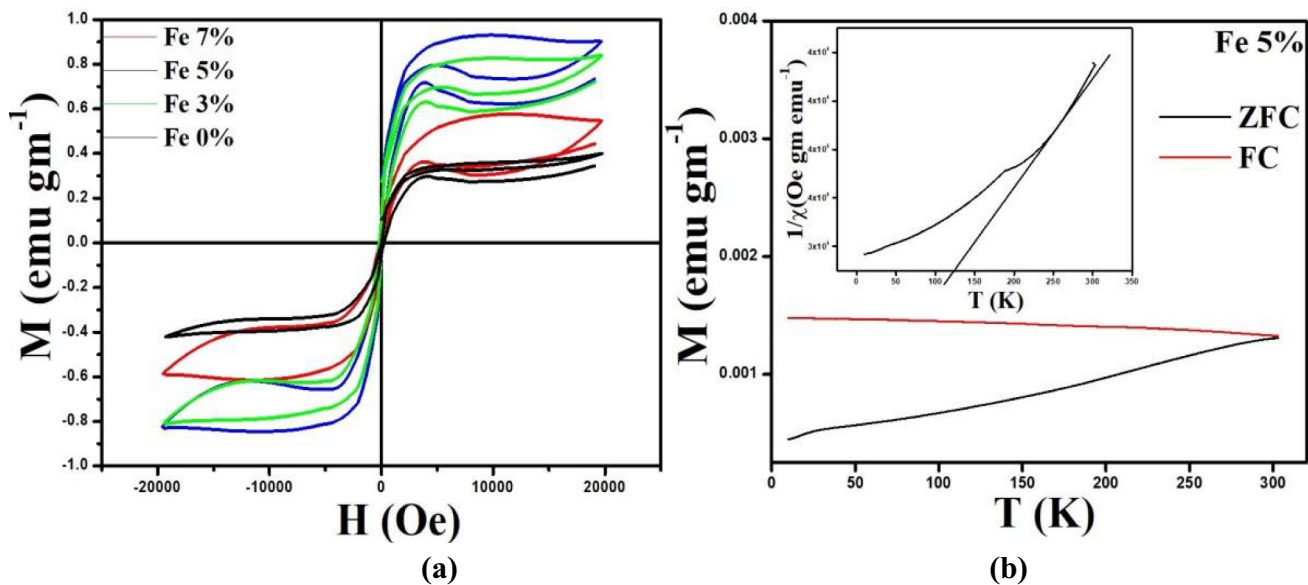


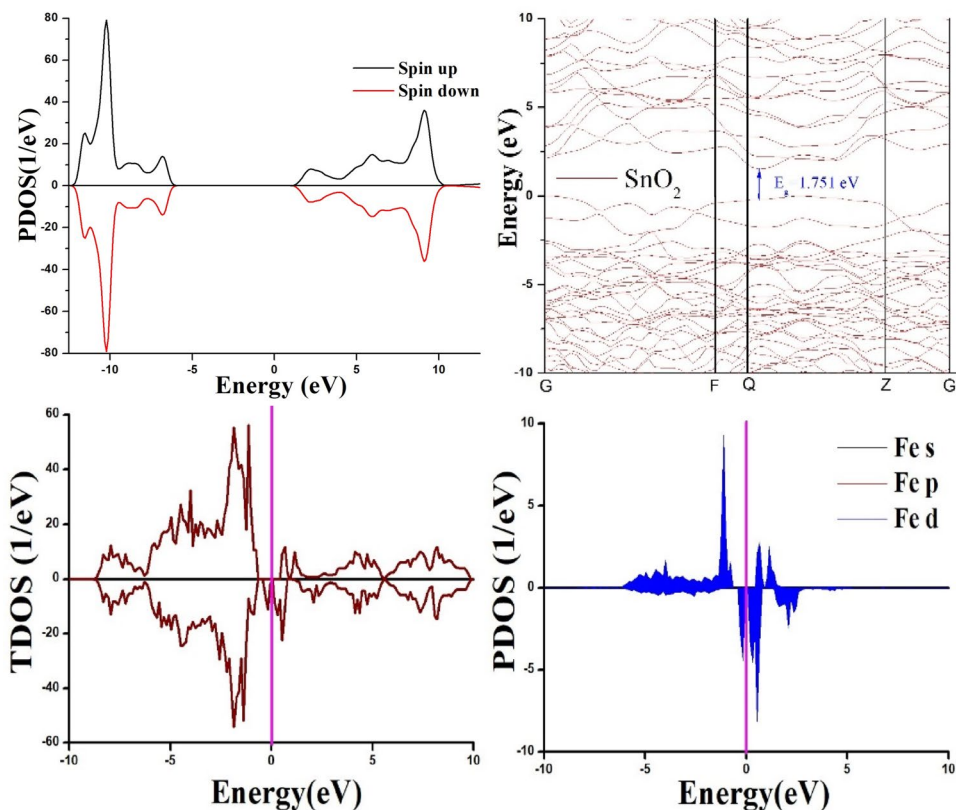
Fig. 5 Variation of Magnetic moment (M) with (a) Applied field (H) for all the samples (b) Temperature (T) for $x=0.05$ of Fe

This is also confirmed from the hysteresis observed at low field as shown in Fig. 5(a). The susceptibility (χ) is obtained using the following equation,

$$\chi = \frac{C}{T - \Theta} \tag{3}$$

where C is the Curie constant, θ is the Curie–Weiss temperature and T is the absolute temperature. The plot of $1/\chi$ Vs. T is shown in the inset of Fig. 5(b). After linear fitting the higher temperature regime and extrapolating the line the value of θ was found to be 125 K. The positive value of θ indicates a ferromagnetic interaction in the system.

Fig. 6 TDOS and PDOS of Fe doped SnO_2



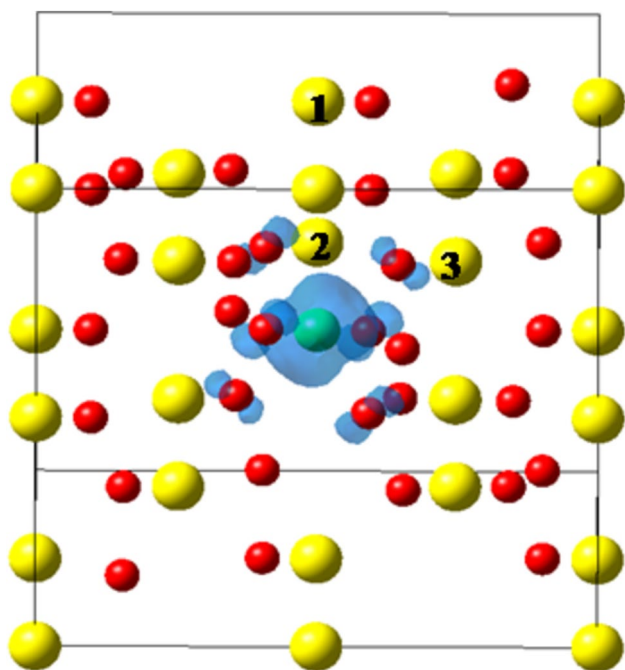


Fig. 7 Spin density distribution for one Fe atom at the center of $2 \times 2 \times 2$ supercell of $\text{Sn}_{16}\text{O}_{32}$, the atoms numbered as 1, 2 and 3 are the three different positions for 2nd Fe atom. Yellow atoms represent Sn, red atoms represent O

The presence of ferromagnetism behavior as observed in Fig. 5(a) can be due to the localized carriers. Oxygen vacancies play an important role in mediating the ferromagnetic exchange coupling between Fe ions. This principle is very consistent with the bound magnetic polarons (BMP) model. The magnetization in this system is a because of correlated spins. The localized spins of Fe can couple to the nearby

F+ center (oxygen vacancy trapping one electron) and convert it to correlated spins [20, 24]. Oxygen vacancies are the ones which give rise to long range ferromagnetic order.

3.4 DFT Investigation

First, to calculate the difference between the structural and optical properties of SnO_2 and Fe- substituted SnO_2 , DFT calculations were performed. $\text{Sn}_{16}\text{O}_{32}$ and $\text{FeSn}_{15}\text{O}_{32}$ supercells were tested with both spin-polarized and spin-unpolarized calculations. The ground state energy for $\text{Sn}_{16}\text{O}_{32}$ was found to be the same in both types of calculation, whereas in $\text{FeSn}_{15}\text{O}_{32}$, the spin-polarized structure was 200 meV more stable than the spin-unpolarized one. Therefore, the spin-polarized structure was considered in both cases to calculate its TDOS (Total Density of States) and PDOS (Partial Density of States) (Fig. 6). The upper part of the valence band is mainly made up of O2p states, while the lower part of the conduction band is dominated by Sn5s states. The contributions from other states such as s, p, and d for Sn and s and p for O are very much negligible compared to that of Fe 3d states. DFT calculations have shown that Fe does create states within the top of the valence band and the bottom of the conduction band. Furthermore, DFT calculations were performed to calculate the difference between the magnetic properties of SnO_2 and Fe-substituted SnO_2 . One Sn atom was substituted by a Fe atom at the center, and then an investigation of the effect on the magnetic property of the system by putting another Fe atom at three different positions named 1Fe, 2Fe, 3Fe, as shown in Fig. 7, was performed. The state of of the 2nd Fe atom was checked. It was found that the antiferromagnetic state is more favorable than the ferromagnetic state at all positions, as shown by ΔE values in Table 2. In this theoretical approach, oxygen vacancies in the Fe-doped

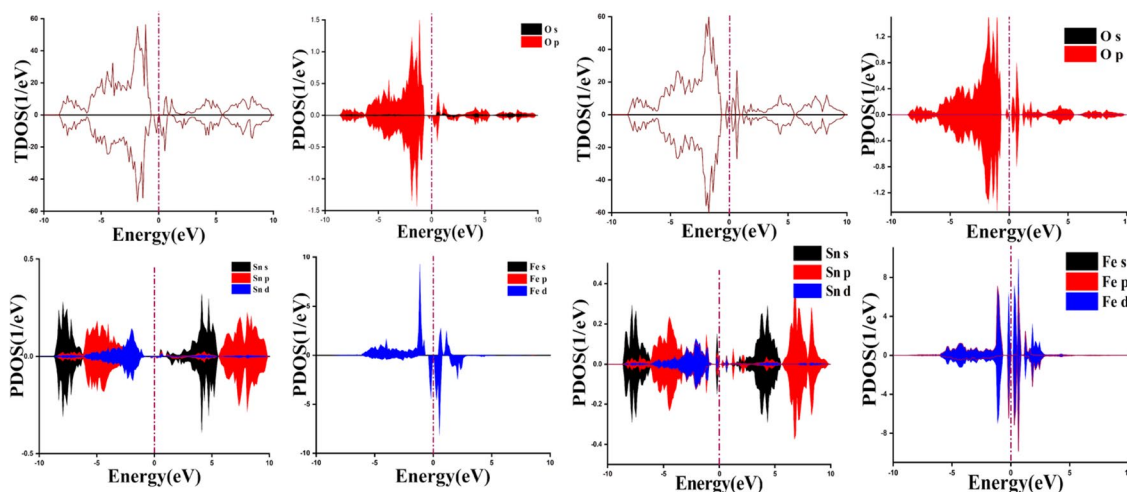


Fig. 8 Total Density of States (TDOS) and Partial Density of States (PDOS) of $\text{Fe}_2\text{Sn}_{14}\text{O}_{32}$ (a) in ferromagnetic state where 1st Fe atom is put at the center while the 2nd Fe atom is put at position 2 (b) in anti-

ferromagnetic state where 1st Fe atom is put at the center while the 2nd Fe atom is put at position 2

Table 2 System, Crystallite Size (nm), Total Magnetization (M_T) in emu gm^{-1} , ΔE (eV) = $E_{\text{AFM}} - E_{\text{FM}}$ (E_{AFM} is the energy of the system in antiferromagnetic state and E_{FM} is the energy in the ferromagnetic state), position of 2nd Fe atom as shown in Fig. 7

System	Crystallite Size (nm)	Total Magnetization (M_T) in emu gm^{-1}	ΔE (eV) = $E_{\text{AFM}} - E_{\text{FM}}$	Position of 2nd Fe atom
X=0.00	12.50	0.031	0.00	
X=0.03	4.66	0.115	-0.01	1
X=0.05	4.27	0.115	-0.19	2
X=0.07	5.03	0.171	-0.45	3

SnO_2 supercell were not considered, which can be studied in future work. However, from the calculation, it can be clearly mentioned that Fe spins do not couple to produce ferromagnetism. They can only form an antiferromagnetic state. This antiferromagnetic state is due to the super-exchange interaction between Fe ions via O^{2-} ions. As it was already stated that the effect of O vacancy in the system was not considered, hence it can be assumed that in the absence of O vacancy, if two Fe atoms are close, then they will form an antiferromagnetic state. The TDOS and PDOS of Fe, Sn, and O states for both ferromagnetic and antiferromagnetic states of 2 Fe are shown in Fig. 8(a) and (b) respectively. A complete dominance of the Fe atom can be seen near the Fermi level (0 eV), which shows that the magnetic property in the theoretical model is governed by Fe. The substitution of two Sn atoms by two Fe atoms in a 48-atom supercell resulted in 12.5% of doping. This doping amount may have crossed the percolation limit (x_p) such that $x > x_p$ and it can also be the reason for the arisen antiferromagnetic state in the above system.

4 Conclusion

In summary, the synthesis of nanocrystalline pristine and Fe-doped SnO_2 nanoparticles via the sol-gel method proved effective, with comprehensive analyses including XRD, HR-TEM, UV-Vis, and PL spectroscopy confirming the substantial impact of Fe doping on morphology, particle size, and band gap properties. Notably, optimal optical characteristics were observed in 5% doped SnO_2 , showcasing Fe 5% doping's superior efficacy, predominantly with Fe atoms substituting at Sn lattice sites, thereby augmenting oxygen vacancies. This heightened substitution, combined with oxygen vacancies, significantly reduced the SnO_2 band gap, rendering it highly promising for optoelectronic device fabrication. Computational simulations unveiled the introduction of Fe3d states near and above the Fermi level upon Fe doping in the SnO_2 supercell, showing limited hybridization with O2p levels. Regarding magnetic properties, both experimental and

theoretical analyses indicated a complex magnetic state in Fe-doped SnO_2 , with potential antiferromagnetic tendencies. Notably, the observed ferromagnetism up to 300 K underscored the material's magnetic potential. Theoretical insights suggested the stability of the antiferromagnetic state over the ferromagnetic state, possibly due to vacancy absence despite limited Fe atoms. In conclusion, iron (Fe) doped tin dioxide (SnO_2) structures present versatile and high-performance materials for diverse applications. With enhanced electrical conductivity, tunable optical properties, magnetic functionalities, and improved catalytic activity, Fe-doped SnO_2 holds significant promise across electronics, optoelectronics, catalysis, and magnetic devices. Furthermore, their enhanced stability and durability underscore their suitability for practical implementation across various fields. Continued research and development in this domain are poised to unlock additional applications and drive further advancements in Fe-doped SnO_2 structures, contributing to the advancement of nanotechnology and materials science, addressing contemporary challenges, and fostering innovation in emerging technologies.

Acknowledgements Author Pawan Chetri would like to acknowledge DST-SERB for funding project bearing file number SUR/2022/003142.

Data Availability The authors confirm that the data supporting the findings of this study are available within the article.

Declarations

Conflicts of Interest The authors declare no competing interests.

References

1. M.A. Kareem et al., Green synthesis of silver nanoparticles (AgNPs) for optical and photocatalytic applications: a review. *Mater. Sci. Eng.* **805**, 012020 (2020)
2. H.S. Akkera et al., Structural, electrical, and optical properties of spin-coated Bi: SnO_2 transparent conducting oxide thin films. *Physica B Condens Matter* **638**, 413839 (2022)
3. H.S. Akkera et al., Structural, electrical, and optical properties of rare-earth Sm³⁺ doped SnO_2 transparent conducting oxide thin films for optoelectronic device applications: Synthesized by the spin coating method, in *Opt Mater (Amst)*, vol. 133, (2022), p.112993
4. A. Uddin, H. Yi, Progress and challenges of SnO_2 electron transport layer for perovskite solar cells: A critical review. *Solar RRL* **6**(6), 2100983 (2022)
5. G. Sun, F. Wang, Y. Zhao, Liquid phase sintering of SnO_2 varistors for stability improvement. *Mater. Chem. Phys.* **305**, 127967 (2023)
6. V. Shah, J. Bhaliya, G.M. Patel, P. Joshi, Room-temperature chemiresistive gas sensing of SnO_2 nanowires: a review. *J Inorg Organomet Polym Mater* **32**(3), 741–772 (2022)
7. C. Wan et al., Inducing the SnO_2 -based electron transport layer into NiFe LDH/NF as efficient catalyst for OER and methanol oxidation reaction. *J. Mater. Sci. Technol.* **124**, 102–108 (2022)
8. K.G. Godinho, A. Walsh, G.W. Watson, Energetic and electronic structure analysis of intrinsic defects in SnO_2 . *The Journal of Physical Chemistry C* **113**(1), 439–448 (2009)

9. L.Z. Liu, T.H. Li, X.L. Wu, J.C. Shen, P.K. Chu, Identification of oxygen vacancy types from Raman spectra of SnO₂ nanocrystals. *J. Raman Spectrosc.* **43**(10), 1423–1426 (2012)
10. J. Li et al., Three-in-one Ni doped porous SnO₂ nanorods sensor: Controllable oxygen vacancies content, surface site activation and low power consumption for highly selective NO₂ monitoring. *Sens Actuators B Chem* **382**, 133550 (2023)
11. D. Rehani, M. Saxena, P.R. Solanki, S.N. Sharma, Transition metal and rare-earth metal doping in SnO₂ nanoparticles. *J. Supercond. Nov. Magn.* **35**(9), 2573–2581 (2022)
12. H.A. Shittu et al., Effect of low-doping concentration on silver-doped SnO₂ and its photocatalytic applications. *Biointerface Res. Appl. Chem* **13**, 165 (2023)
13. C. Afonso et al., Effect of Iron-Doping on the Structure and Photocatalytic Activity of TiO₂ Nanoparticles. *Catalysts* **13**(1), 58 (2022)
14. F. Irfan, M.U. Tanveer, M.A. Moiz, S.W. Husain, M. Ramzan, TiO₂ as an effective photocatalyst mechanisms, applications, and dopants: a review. *Eur. Phys. J. B.* **95**(11), 184 (2022)
15. K.K. Pandimeena, M.C. Robert, S. Saravanakumar, Energy gap tuning, ferromagnetic switching, visualization of electron density and bonding in dilute magnetic semiconductor Fe-doped SnO₂, in *Optik (Stuttg.)*. (2023), p.171091
16. S.M. Yakout, Room temperature ferromagnetism: nonmagnetic semiconductor oxides and nonmagnetic dopants. *J. Electron. Mater.* **50**(4), 1922–1941 (2021)
17. I. Lungu, A.M. Grumezescu, C. Fleaca, Unexpected ferromagnetism—A review. *Appl. Sci.* **11**(15), 6707 (2021)
18. N. Shukla, P. Chetri, G.A. Ahmed, Structural, optical and magnetic study of Eu²⁺ doped SnO₂ nanosystems: an experimental and DFT based investigation. *J. Mater. Sci.* **56**(34), 18911–18925 (2021)
19. P. Chetri, B. Choudhury, A. Choudhury, Room temperature ferromagnetism in SnO₂ nanoparticles: an experimental and density functional study. *J. Mater. Chem. C* **2**, 9294–9302 (2014)
20. R.E. Vizhi, R. Rajan, Structural, optical and room temperature magnetic properties of sol–gel synthesized (Co, Fe) co-doped SnO₂ nanoparticles. *J. Cryst. Growth* **584**, 126565 (2022)
21. A.B. Ali Baig, V. Rathinam, V. Ramya, Synthesis and investigation of Fe doped SnO₂ nanoparticles for improved photocatalytic activity under visible light and antibacterial performances. *Mater Technol* **36**(10), 623–635 (2021)
22. P.V. Jithin, K. Sudheendran, K.J. Sankaran, J. Kurian, Influence of Fe-doping on the structural and photoluminescence properties and on the band-gap narrowing of SnO₂ nanoparticles, in *Opt Mater (Amst)*, vol. 120, (2021), p.111367
23. Y. Gao, Q. Hou, Q. Liu, First-principles study on the electronic structures and magneto-optical properties of Fe^{2+/3+} doped SnO₂. *Solid State Commun.* **305**, 113764 (2020)
24. D. Manikandan, R. Murugan, Genesis and tuning of ferromagnetism in SnO₂ semiconductor nanostructures: Comprehensive review on size, morphology, magnetic properties and DFT investigations. *Prog. Mater. Sci.* **130**, 100970 (2022)

Publisher's Note Springer Nature remains neutral with regard to jurisdictional claims in published maps and institutional affiliations.

Springer Nature or its licensor (e.g. a society or other partner) holds exclusive rights to this article under a publishing agreement with the author(s) or other rightsholder(s); author self-archiving of the accepted manuscript version of this article is solely governed by the terms of such publishing agreement and applicable law.